ADAPTIVE TECHNIQUE FOR RADIATION PATTERN SHAPING OF PARABOLIC MESH ANTENNAE: A LOW COST APPLICATION OF SMA ACTUATORS IN SPACECRAFT

O. de Weck, D. Miller, J. Hansman
Department of Aeronautics and Astronautics
Massachusetts Institute of Technology, Cambridge, USA

Abstract

The area of satellite communications in the RF spectrum has gained increased importance over the last decade. Several trends have emerged, which focus on rapidly changing RF energy illumination requirements. A novel technique for low-cost shaping of parabolic antenna patterns in space is presented. Shape Memory Alloy (SMA) wire actuators are used to control the shape of a parabolic center-feed reflector designed for a carrier frequency of 12 GHz. Based on temperature and displacement measurements of a 8-inch testbed reflector, a finite element model and a planar dipole array approximation, the actuation bandwidth and antenna pattern modulation is predicted. A bandwidth of up to 0.2 Hz, sidelobe modulation of 8 dB and boresight axis slewing up to 4° can be achieved at a fraction of the cost of phased array or multiple feed systems.

Introduction

Satellite communications technology has evolved at a dramatic pace over the last decade. While phased array systems allow beam steering and beam forming capabilities, the use of phased array technology in space has been somewhat limited. The reasons are the high weight, complexity and cost of phased array systems [1]. The findings of this project show a new and low-cost approach to antenna radiation pattern shaping using SMA wire actuators.

Due to the high path losses, up to 200dB for a geosynchronous orbit, typically the desired radiation pattern for point-to-point communications is a single narrow beam (main lobe) [1]. For transmission of RF power to several ground stations at the same time or for a specified ground coverage, the requirements are more complex. In those situations multiple beams or a prescribed gain footprint on the earth surface are paramount. Traditional engineering solutions have focused on multiple off-center feed arrays or asymmetric shaping of reflector surfaces. The latter option has been successfully implemented for GEO satellites, which are optimized for coverage of specific land masses. Once a "fixed-shape" reflector antenna is deployed on orbit, however the radiation pattern can no longer be modified. This is where a SMA adaptive antenna, such as the one in figure 1, can provide a technological advantage. Depending on the desired footprint, a controller activates the distributed SMA actuators until the demand changes again. It is the objective of this paper to lay out the analysis steps, which allow a quantification of the expected performance of such an approach.

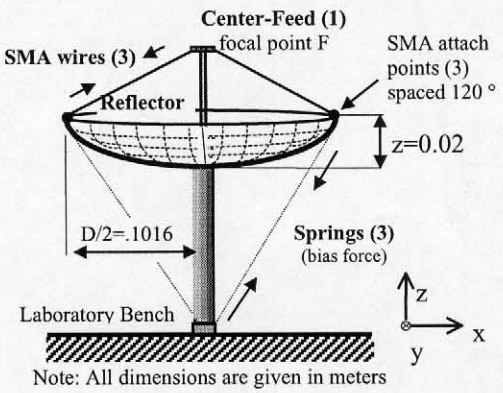

Fig. 1: *8 inch -Parabolic SMA- Mesh Antenna*

Problem Formulation and Methodology

The main problem is to develop a methodology for predicting the performance of high gain antennas, which are actuated by SMA wires acting on the periphery. Figure 2 shows the analytical and experimental steps of our approach. An input voltage U_o creates a temperature change through resistive heating of the SMA actuator (step 1). The subsequent phase transformation is governed by the nonlinear SMA constitutive laws and leads to measurable displacements at the mesh attach points (step 2). From the recorded time histories important conclusions about the actuation bandwidth and stroke of the antenna are drawn.

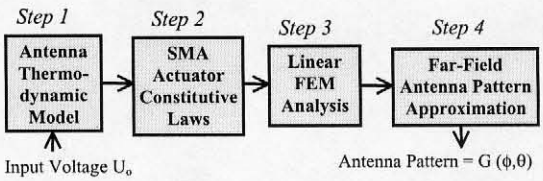

Fig.2 *Diagram of experimental and analytical procedure*

Steps 1 and 2 are validated experimentally. Then the attach point displacements are used as applied static

loads to a finite element model (FEM) of the mesh antenna structure (step 3). The projection of the displaced nodes onto a circular exit aperture can be interpreted as a planar array of dipoles. This perturbation method is commonly used for the approximation of far-field antenna patterns as a multi-element array (step 4). This yields the data necessary to assess the effectiveness of the approach. The four key questions are:

1. *What is the expected performance in terms of beamwidth modulation, boresight axis slewing, and first side lobe gain modulation?*
2. *What SMA actuation bandwidth can be achieved under laboratory conditions ?*
3. *What are the challenges for the closed loop control of a SMA-parabolic reflector antenna ?*
4. *How does this compare to phased arrays ?*

Shape Memory Alloy Actuator

A NiTi alloy with properties according to table 1 was chosen for this application.. The consideration of SMA's for space applications is based on the high work density and reliability compared to traditional mechanisms. Cycling fatigue of SMA actuators has been described by various authors [4]. The SMA alloy composition is very important for use in space due to the large temperature gradients and temperature changes which are experienced by the satellite hardware. The contraction is due to the phase transition from martensite α to austenite β. The contraction speed depends on the current $I_o(t)$.

Property NiTi	d=150 µm wire
Young's Modulus E_{mart} [GPa]	28
Specific Resistance R [Ω/m]	75
Latent Heat [J/kg]	24,200
Activation Start and Finish T	A_s=68°C , A_f=78°C
Relaxation Start and Finish T	M_s=52° , M_f=42°C

Table 1: *Nitinol wire properties*

Once the phase transformation is complete (ξ=1) we have 100% α and U_o can be reduced in order to maintain a thermal equilibrium temperature above A_f [4]. This maintains the contracted length $l_o(1-\varepsilon)$. After a further reduction of the input voltage U_o, the wire cools down due to free convection to air and conduction through the attach points. The cool down period is determined by the equilibrium temperature T_o and the thermal boundary conditions. A rigorous model of this process was developed. An undesirable fact of SMA wire actuators is that a bias force needs to be applied by springs, in order to return to the original length l_o. The potential for two-way-shape memory (TWSM) exists; this however requires "training" of the wires as demonstrated by White and Hebda [5]. Nitinol wires can also be damaged by overheating. If the critical temperature T_c =250 °C is exceeded the annealing process is started and the shape memory is "erased" by setting the alloy to the new configuration. This has to be avoided by judiciously controlling the input voltage. The benefits of using SMA wire actuators for this application are:

- small size and light-weight actuator
- low power consumption for small diameters
- large force and/or strain output per volume
- electrical actuation at low voltage levels[1]

Thermomechanical Model of SMA Actuator

The thermodynamics of the wire are modeled as a transient heat transfer with T= f (x, r_o, θ, t). A simplification is offered by the "lumped" body approach. The test for this assumption is provided by the Biot-Number. For a cylindrical body of length l_o and radius r_o , where $l_o >> r_o$,it is given as:

$$Biot\# = \frac{h_c \cdot r_o}{k} = 2.68 \cdot 10^{-4} \qquad \{1\}$$

where h_c[2]is the convection coefficient in [W/m^{2}K], r_o is the wire radius in [m] and k is the thermal conductivity in [W/mK]. The free convection for a thin wire has been described in detail by Kreith and Bohn [6]. The Biot # is lower than the 0.1 limit and it is acceptable to use the "lumped" body approach. The terms contributing to the thermal balance of the SMA actuator are shown in figure 3.

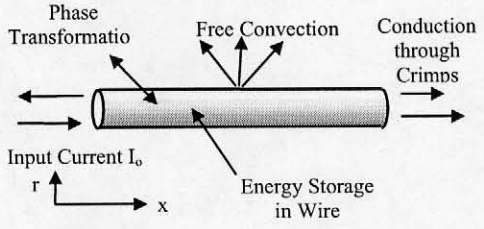

Fig. 3 : *Thermal balance of SMA wire actuator*

Electrical Power Input:

$$P_{in} = \int_l U_o^2(t)\frac{1}{R}dl = \frac{U_o^2(t)}{Rl} \qquad \{2\}$$

Free convection from wire:

$$q_h = \iint_A h_c(T(t) - T_o)dA \qquad \{3\}$$

Energy storage in body:

$$q_c = \iiint_V \rho c_p \frac{dT}{dt}dV \qquad \{4\}$$

[1] SMA's can be actuated around 1-10 VDC compared to piezoceramics, which require higher voltages. This is a key advantage for use in space, where the power is usually generated by solar arrays at 24 ~ 28 VDC.

[2] Estimated values for h_c are 26-40 [W/m^{2}K].

Conduction through ends:

$$q_k = 2 \cdot \iint_A \frac{k}{\chi}(T(t_o) - T)dA \qquad \{5\}$$

Phase transform and work output:

$$q_\xi = \iiint_V \frac{d\xi}{dT} \cdot \frac{dT}{dt} \cdot (Q_{ph} + W_o)dV \qquad \{6\}$$

With the first term {2} on the right side and the other terms on the left side, we can rearrange and obtain a first order differential equation and write:

$$(\alpha + \beta(T))\frac{dT}{dt} + \gamma T - \gamma T_o = \delta U_o^2(t) \qquad \{7\}$$

where the coefficients are constant with the exception of β, which is temperature dependent. For this reason the ODE cannot be solved explicitly. An iterative scheme for arbitrary input voltages Uo was implemented. For a square pulse input the expected transient response is shown in figure 4. It seems that the step introduced by the phase transformation is somewhat overpredicted by the model. The rise and cooling times however match reasonably well.

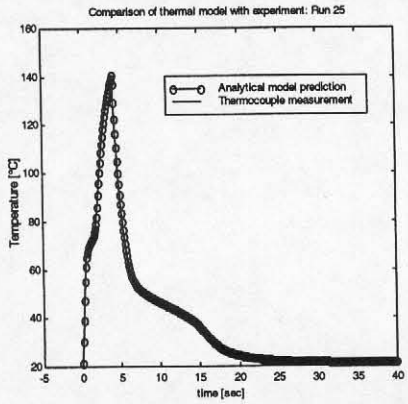

Fig.4: *Comparison of model prediction and recorded SMA temperature , voltage U_o=2.5V, t_1=4.0 sec*

For a uniaxial SMA the constitutive equation are:

$$\sigma = D\varepsilon + \Theta T + \Omega\xi \qquad \{8\}$$

where the state variables and properties are

σ: Stress [Pa]
ε: Strain [-]
T: Temperature [K]
ξ: Martensite fraction
D: Elastic Modulus [Pa]
Θ:Thermoelastic Tensor [Pa/K]
Ω:Transform Tensor [Pa]

The Modulus and the two tensors are each a function of strain, martensite and temperature. The martensite fraction is the chosen state variable that drives material transformation. The Liang and Rogers cosine and exponential models, the Tanaka and Brinson models were explored (step 2) [5].

Antenna Testbed Architecture

The RF carrier frequency of the antenna system was chosen to be f_c = 12 GHz, which corresponds to a wavelength of λ = 1 inch (2.54 cm). RF Design experience dictates that the parabolic reflector diameter has to be at least 5-10 times the wavelength λ [7], so that a diameter of 8 inches (=20.32cm) was chosen for the experimental setup. The antenna is clamped at the inner radius and has a mesh size of 1mm. Three SMA wire actuators with a length of 100mm each and a diameter of 150μm are attached at the focal point at one end and equally spaced by 120° at the periphery of the mesh on the other end. Elastic springs are used to provide the necessary bias force (figure 5).

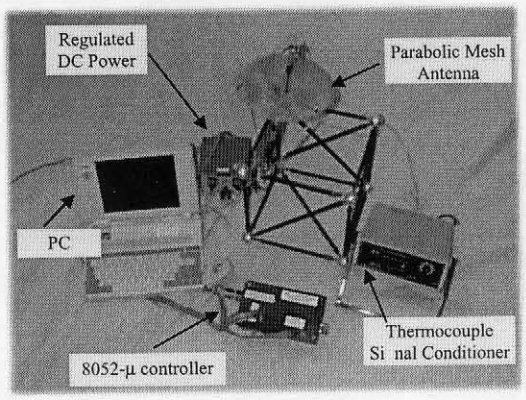

Fig. 5: *Testbed for parabolic antenna reflector*

In order to study the effects of various pulse inputs into the SMA actuators a 8052 μ-controller IC with RS-232 serial interface was chosen. A 0.0005" foil thermocouple with a time constant τ =0.27 sec recorded the wire temperature at the midpoint. A semiconductor 3B-class laser is used as a displacement sensor at the attach points. Nyquist sampling at 20 Hz or 50 Hz provided time domain samples of 81.92 and 32.77 seconds respectively.

Experimental results

The cycling period T, the duty cycle dc and the voltage level Uo are varied according to a 56 point test matrix. For a short duty cycle and high voltage the input looks like an impulse. Figure 6 shows the time history results for a typical intermediate case. The three traces represent the input voltage, displacement of SMA attach point and thermocouple temperature. After analyzing the time traces, three types of thermal responses are possible in terms of the peak temperature of the SMA wire:

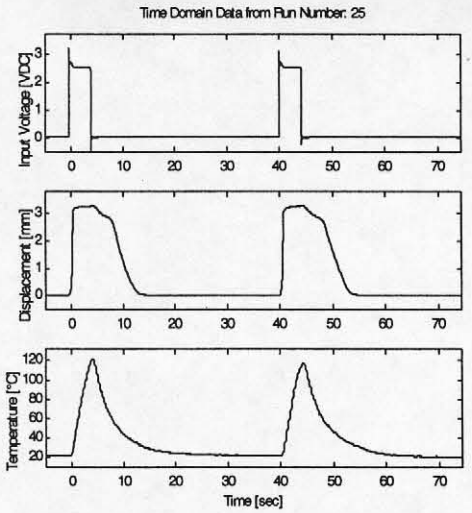

Fig. 6: *Time traces for T=40 sec, dc = 10%, U_o=2.5 V*

Overheating: For an impulse-like input at high voltage the temperature increases very rapidly and exceeds the critical level Tc = 250°C.

Nominal Range: This is the desirable response for a square pulse input which results in complete phase transformation without exceeding Tc.

Cool Range: The energy is "spread" out too much and a thermal equilibrium is reached, which is below the transition temperature A_f.

These three regions are shown in figure 7. Thermal equilibrium is reached in all cases after 6 seconds. The higher the input voltage, the longer it takes to reach equilibrium. Actuation is not possible for voltages below 1.5 V. For voltages above 3.2 Volts, the pulse length has to be limited because the equilibrium temperature exceeds 250°C.

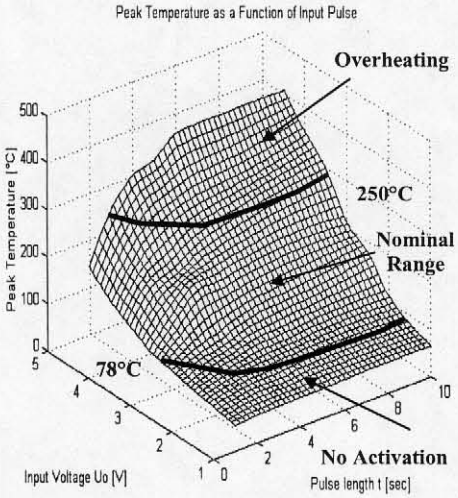

Fig. 7: *Measured Regions of SMA operation*

If the wire actuator is cycled faster (T is reduced), saturation will occur. This happens when a new pulse is generated before the wire temperature has had time to drop below M_f. The data indicates that the fastest pulse repetition frequency (PRF), which can be achieved with full phase cycling is around 0.2 Hz (T=5 sec). This is the actuation bandwidth under laboratory conditions. The expected hysteretic behavior (based on manufacturer data, see table 1) was confirmed. Figure 8 contains a comparison of the measured and predicted hysteresis curves.

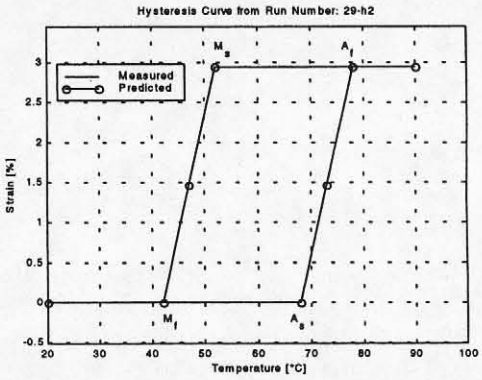

Fig. 8: *Hysteresis curve of 150-μm SMA wire (NiTi)*

Pulse Width Modulation (PWM) is proposed for active control of the actuator. This power-efficient technique inputs energy into the actuator by varying the duty cycle and period and acting as a double oscillator [4]. Fig. 9 shows that PWM can maintain the fully actuated position without overheating and can also generate intermediate positions.

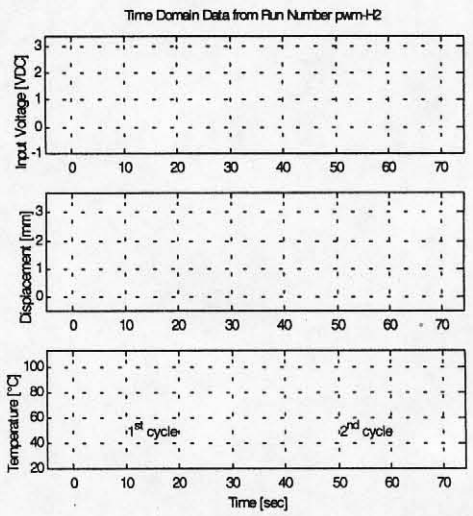

Fig. 9: *PWM-control of SMA wire actuator*
1st cycle: t_{cool}=0.733 sec, 2nd cycle: t_{cool}=0.37 sec

Linear Elastic Finite Element Model

A finite element model of the parabolic reflector was generated with ANSYS. The mesh model consists of a total of 324 nodes and uses isoparametric triangular and quadrilateral shell elements. The boundary conditions clamp all nodes on the inner annulus circumference. The loading occurs by prescribing the three measured SMA wire attach point displacements. The maximum displacement of 3.25 mm is used. The linear elastic

results for the nodes along the primary meridian - as indicated in figure 10 - are used to compute the antenna pattern.

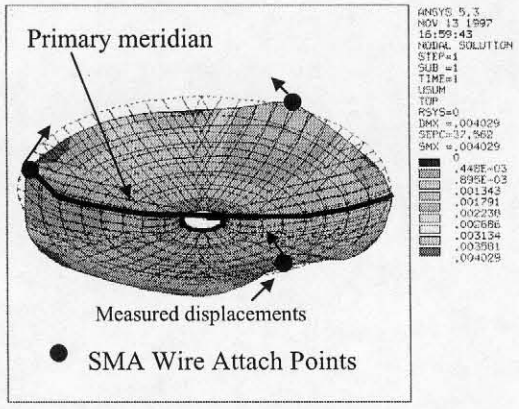

Fig. 10 *Linear elastic FEM of active antenna*

Antenna Pattern Far Field Approximation

A method to evaluate the far-field pattern of an adaptive antenna based on Fourier transforms of the surface current distribution was presented by Washington [8]. It is also possible to approximate the far-field radiation pattern of an antenna by a multi-element planar array of dipoles [2]. This perturbation method was chosen in this project. The pattern of such an array can be obtained by adding vectorially the field strengths due to each of the radiating elements. If the spacing between elements d is much smaller than the distance r to a point A, the far-field approximation is valid. The electric field at point A due to an arbitrary element i is :

$$\overline{E_i} = f(\theta,\phi)\frac{e^{-j\cdot\beta_o r}}{(r_o + id\cos\theta)}e^{j\beta_o id\cos\theta} \qquad \{9\}$$

The electric field strength at A can be calculated as a superposition of the signals arriving from each dipole. We can thus write:

$$\overline{E_T} = f(\theta,\phi)\frac{e^{-j\beta_o r_o}}{R}\left[1+\sum_{i=1}^{N-1} c_i e^{j(\beta_o id\cdot\cos\theta\alpha_i)}\right] \{10\}$$

The term in brackets is termed the "array factor" Γ and is a measure of the far-field pattern as a function of the Euler angle θ. For a perfectly symmetric parabolic reflector, the phase shift α_i between elements is zero, as all rays emanating from the center-feed focal point F, reach the imaginary exit aperture at the same time. In that case the array factor Γ in equation {10} can be simplified to:

$$|\Gamma| = \frac{\sin\left(\frac{N}{2}\right)\left(\beta_o d\cos\theta\right)}{\sin\left(\frac{1}{2}\right)\left(\beta_o d\cos\theta\right)} \qquad \{11\}$$

where N is the number of dipoles. For a perfectly rotationally symmetric parabolic antenna the gain G_o can be calculated from the frequency f in GHz, the antenna diameter D in meters and the efficiency η=0.55 [1], which yields:

$$G_o = \frac{\pi^2\cdot D^2\cdot\eta}{\lambda^2} = 358.6 = 25.55dB \qquad \{12\}$$

The simplifications which led to equation {11} are no longer valid in the general case. Therefore a numerical solution including the phase shift α_i for each array element was developed. The projection of each node of the FEM onto the exit aperture may be considered as an element of the planar dipole array. From the position vector field of the displaced nodes, a phase shift α_i can be computed for every node on the reflector surface. Figure 11 shows the displaced configuration and {13} is the equation for phase shift calculation.

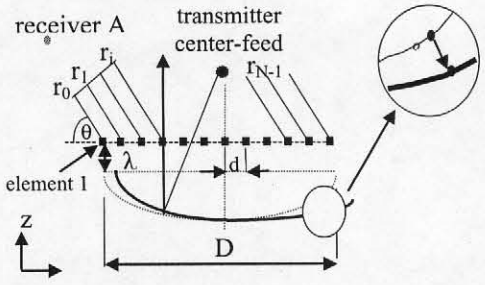

Fig.11: *Perturbed reflector surface approximation*

$$\alpha_i = \frac{\bar{r}_i - \bar{r}_o}{\lambda}\cdot 2\pi \qquad \{13\}$$

A small angle assumption has been made in that the only factor affecting α_i is the path difference due to the perturbed surface from the focal point F to the radiating element i. Finally figure 12 shows the perturbed radiation pattern for the SMA-actuated antenna. This is the radiation pattern along the primary meridian as defined in figure 10. It can also be interpreted as the radiation pattern evaluated in the vertical plane containing the antenna boresight axis and one SMA attach point.

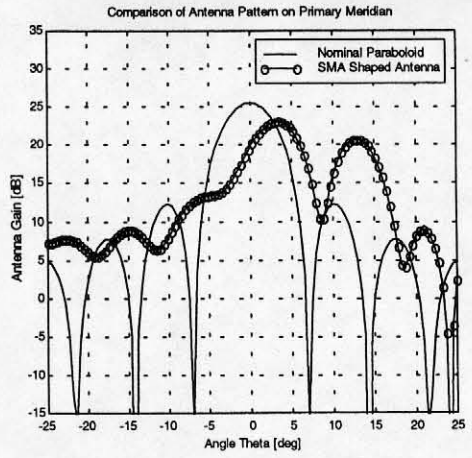

Fig.12: *Comparison of nominal and shaped antenna pattern along primary meridian*

It can be verified that shaping the antenna surface has had several pronounced effects on the far-field pattern. This result is valid for the specific configuration as described in this paper.

Conclusions for Antenna Performance

It has been shown that the reflector antenna surface can be shaped with the help of SMA actuators acting on the mesh periphery. This shape change affects the far-field radiation pattern and provides the data necessary to answer the four key questions.

1. Expected Performance

Boresight axis slewing: The peak gain is no longer at $\theta=0°$ but has been shifted to + 4°.

Main lobe peak gain: The peak gain (principal maximum) is reduced from 25.6 dB to 23.2 dB

Beamwidth spreading: The -3dB beamwidth is enlarged from 7° to 8.5°

Beam pattern shaping: The first side lobe on the right has shifted and changed in magnitude by 8dB

If such an antenna would be on an earth orbiting satellite, clearly we would also have affected the footprint onto earth's surface, which is now no longer representative of a simple spot beam.

2. Actuation bandwidth

The data indicates the fastest pulse repetition frequency (PRF) without reaching saturation to be around 0.2 Hz. This is the actuation bandwidth under laboratory conditions. The bandwidth under space conditions would be different due to radiation heat transfer (Stefan-Boltzmann law).

3. Challenges for closed loop control

The main challenges for closed loop feedback control of a PWM actuated parabolic reflector surface with SMA's are summarized as follows:

- The actuator control model has to take into account the hysteresis effect (Preisach model)
- Simple PID-controller can be implemented with displacement and rate feedback
- Most temperature sensor are not suitable for feedback due to large time delay τ
- Good thermal model of SMA actuators and environment (see below) is needed

For use in space, the thermal environment of the SMA component has to be known with a good degree of accuracy. It has to be ascertained that the device is not activated accidentally, i.e. the operating temperature always remains below A_s.

4. Comparison to Phased Array Technology

This approach can be implemented for LEO and MEO communication antennas which modify their shape in order to meet specified and changing RF power transmission requirements during orbit. Key advantages of this method are low costs and the ability to control even large, low-area-density devices. Phased array antennae are still more advantageous if several distinct beams or rapid electronic beam steering is required. This capability however comes at a higher cost, complexity and weight penalty compared to the lightweight adaptive antenna reflector presented in this project.

Recommendations for future research include actual measurements of far-field antenna patterns in anechoic chambers, precision modeling of radiation patterns with 3D-Maxwell solver and closed loop PID control experiments of the active antenna. As an ultimate goal it is desirable to prescribe a desired RF footprint and deduce the corresponding actuation sequence.

References

[1] Larson W., Wertz J.R., "Space Mission Analysis and Design" , Second Edition, Microcosm Inc., 1992

[2] Fogiel, M, "The Electronic Communications Problem Solver ", Chapter 18, "Antennas", Research and Education Association, New York, NY, 10018,1988

[3] Jackson, C.M. e. a., "55-Nitinol - The alloy with a memory" , NASA SP-5110, Washington DC, 1972

[4] Gilbertson R.G., "Muscle Wire Project Book" , Third Edition, Mondo-Tronics Inc., 1994

[5] Hebda D. A., White S.R ., "Hysteresis Testing of Nitinol Wires", AD-Vol. 45, Adaptive Structures and Composite Materials Analysis and App., ASME, 1994

[6] Kreith, F. and Bohn M. S., "Principles of Heat Transfer", 4th ed., Harper & Row Publishers, NY, 1986

[7] Evans, A.J., Britain, K.E., "Antennas - Selection, Installation and Projects", 3rd ed., Master Pub., 1994

[8] Washington, G. " Smart Aperture Antennas", SPIE Vol. 2722, p. 189-196